Flow Past V-Groove Circular Cylinders

N. W. M. Ko,* Y. C. Leung,† and J. J. J. Chen‡
University of Hong Kong, Hong Kong

Measurements of the mean pressure distributions and Strouhal numbers on six V-groove circular cylinders and a smooth circular cylinder were made over a Reynolds number range of 2×10^4 to 1.6×10^5. Spectra of the velocity fluctuations downstream of the cylinders were also measured. The transition from subcritical to critical and from critical to supercritical flow regimes occur at lower Reynolds numbers for the V-groove cylinder than for the smooth cylinder. However, when the Reynolds number is based upon an equivalent diameter, which represents the total surface area of the cylinder, it is found that the Reynolds number trends are very nearly the same for V-groove and smooth cylinders.

Nomenclature

C_p = pressure coefficient $(p - p_0)/q_0$
C_{pb} = base pressure coefficient
C_{pm} = minimum pressure coefficient
d = diameter of cylinder
d_{eq} = equivalent diameter, $(1 - h/d)d/\sin(\phi/2)$
h = depth of V-groove
k_s = roughness
ℓ = length of cylinder
p = static pressure
p_0 = freestream static pressure
q_0 = dynamic pressure of freestream
Re = Reynolds number, $V_0 d/\nu$
Re_{eq} = equivalent Reynolds number, $V_0 d_{eq}/\nu$
St = Strouhal number, fd/V_0
V_0 = freestream mean velocity
u = streamwise velocity fluctuations
x, y, z = streamwise, lateral, and spanwise coordinates, respectively
ν = kinematic viscosity
σ_u = rms value of u
ϕ = angle of V-groove
θ_i = angle of inflexion point of pressure distribution
θ_m = angle of minimum pressure coefficient
θ_w = angle at the beginning of the wake region

Introduction

THE drag and heat-transfer characteristics of a flat surface with longitudinal ribs of rectangular, triangular, and transversely curved shapes have been investigated.[1,2] The purpose of the longitudinal fins was to confine the turbulent bursts to regions having small transverses. In this way, it was hoped to alter the local turbulence production and thereby the drag. However, it was found that whether the drag increases or decreases depended on the configurations of the ribs, such as the height, spacing, and shape. For a V-groove surface, drag reduction was measured for depths $h^+ < 25$ and spacings $s^+ < 200$ in terms of the law of the coordinates. The reduction was associated with a decrease of momentum thickness, turbulent velocity fluctuations, and Reynolds stresses. The above investigations were all made at zero pressure gradient.

For flows with pressure gradients, the surface roughness of a circular cylinder has been found to affect the vortex shedding, drag, and heat-transfer characteristics.[3-7] The effects of surface roughness on the flow in the subcritical, critical, supercritical, and transcritical Reynolds number regimes were investigated. It was found that surface roughness promoted boundary-layer transition and significantly affected the subsequent flow development at Reynolds numbers higher than the critical. Generally, the drag coefficient and Strouhal number of rough cylinders varied with the Reynolds number in a way similar to those of a smooth cylinder, an increase in surface roughness moving the curves toward lower Reynolds numbers. This progressive shift was associated with an increase in the minimum drag coefficient. The drag coefficient, the base pressure coefficient C_{pb}, and the pressure recovery $C_{pb} - C_{pm}$ were all found to correlate well with a parameter based on surface roughness and Reynolds number.[6,8] The artificial transition of the boundary layer by surface roughness and the associated progressive shift toward lower Reynolds numbers provided a means of producing effective high Reynolds number flow at relatively low Reynolds numbers. In the investigations cited above, the surface roughness was created by using commercial sandpaper of varying grades,[4] polystyrene particles for coarse roughness and sandpaper for fine roughness,[6] and pyramidal surface roughness produced by a knurling process.[5] In the last investigation, the surface roughness was not of a random nature, as in the case of the other two.

In view of the lack of information about a circular cylinder with ribs on its surface, the present investigation to study the effect of the streamwise V-grooves on the flow was undertaken. It was hoped that this study would provide an insight into the possible use of V-grooves for drag reduction. Instead of crude control by trip wires and induced transition to different flow regimes by rough elements, it was hoped that the study might offer more exact control and a better understanding of the mechanism involved in the induced transition of cylinder flows. Different V-groove configurations were examined in a Reynolds number range within the subcritical Reynolds number regime of a smooth cylinder.

Experimental Arrangements

The experiments were carried out in a wind tunnel with a test section measuring 56 × 56 cm. The freestream turbulence intensity was about 0.4% at 22 m/s. Most of the tests were carried out with cylinders having a diameter of 48.8 mm. A cylinder of larger diameter, $d = 101$ mm, was also studied in a higher Reynolds number range. The blockage ratio for the

Received Dec. 9, 1985; revision received June 30, 1986.

*Reader, Department of Mechanical Engineering.
†Research Student, Department of Mechanical Engineering.
‡Lecturer, Department of Mechanical Engineering; presently Lecturer, Department of Chemical and Materials Engineering, University of Auckland, New Zealand.

smaller cylinder was 9%, while that of the bigger cylinder was 18%. The effect of blockage ratio was corrected by applying the formulas of Allen and Vincenti.[9] For both cylinders, end plates were used to eliminate the effect of the tunnel boundary layers. The respective aspect ratios ℓ/d for the small and large cylinders were 9 and 4.4. In addition, a smooth cylinder of 48.8 mm diameter was also examined for comparison. The effect of aspect ratio, particularly the low aspect ratio of the large cylinder, is being studied in another investigation and will be reported later. The range of Reynolds number for the small cylinders was about $2–7.3\times10^4$ and for the big cylinder about 4×10^4 to 1.6×10^5. Both ranges are within the subcritical Reynolds number regime of smooth cylinders.

The V-groove configurations studied are shown in Fig. 1 and tabulated in Table 1. Because of the small dimensions involved, it was difficult to obtain identical configurations of the V-grooves across the span of the cylinder. The dimensions shown in Table 1 were the averaged results of a few samples of the V-groove. Three pressure taps were located at three different spanwise positions on the cylinder: at the midsection and at 10 and 20 mm from it (Fig. 1). The pressure taps had an inner diameter of 0.6 mm and were centered in the V-groove. However, because of the small dimensions of the V-grooves, the pressure taps in many cases covered more than one groove (see Table 1). The cylinder was rotated to obtain the circumferential pressure distribution.

From the mean static pressure distribution, the base pressure coefficient C_{pb}, the minimum pressure coefficient C_{pm}, the location θ_m of the minimum pressure coefficient, and the approximate location θ_w of the beginning of the wake region were also determined.[4,10] All of the pressure coefficients were corrected for blockage. The drag coefficient C_d was calculated from the integration of the pressure distribution around the whole cylinder.

For the measurements of the velocity fluctuations downstream of the cylinder, a cross-wire probe was used to measure the streamwise u component. The wires have a diameter of 5×10^{-6} m and working length of 2 mm. The hot-wire anemometer was of a constant-temperature type. The cross wire was located at $x/d=2$ and $y/d=\pm0.5$ and its signals were spectrally analyzed by a Hewlett Packard structural dynamics analyzer, type 5423A. The Strouhal number of the vortex wake thus obtained was not corrected for blockage.

Results and Discussion

Figure 2 shows some of the static pressure distributions measured on the cylinders at location A, that is, at the center of the wind tunnel, at a Reynolds number of 7.2×10^4. The distribution on the smooth cylinder at the same Reynolds number is also shown. Even though the flow at this Reynolds number is within the subcritical regime of a smooth cylinder,[11–13] the pressure distributions on the V-groove cylinders are significantly different from that on a smooth cylinder. The pressure distribution on model 6 even indicates asymmetric flow, with an inflexion point on one side only at $\theta_i\approx80$ deg. The occurrence of asymmetry and an inflexion point, which indicates laminar separation and turbulent reattachment forming a separation bubble, has been observed in the critical regime of a smooth cylinder,[13–15] the inflexion point occurring at $\theta_i\approx90$ deg.

The effect of the Reynolds number on the pressure distribution at the midsection (location A) of model 11 is shown in Fig. 3. Large variations in the distribution are found over the Reynolds number range of $3.0\times10^4\le Re\le7.2\times10^4$. Further, asymmetry is found at Reynolds number of 5.3–6.0 $\times10^4$. At the latter Reynolds number, an inflexion point occurs at $\theta_i\approx80$ deg.

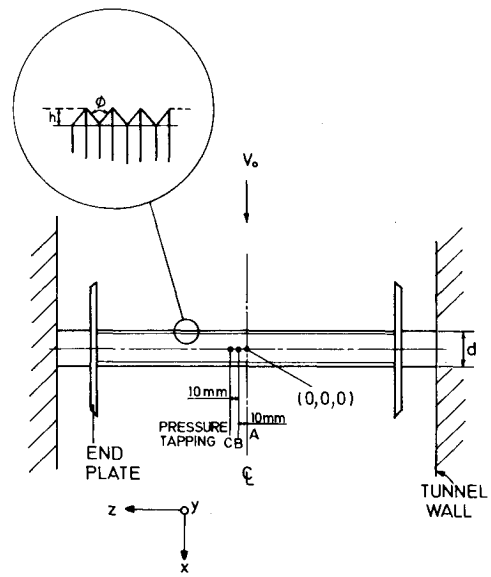

Fig. 1 Schematic diagram of V-groove circular cylinder.

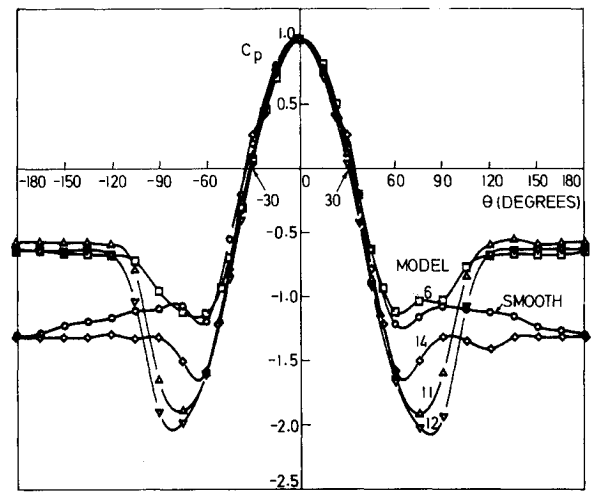

Fig. 2 Pressure distributions on cylinder at $Re=7.2\times10^4$.

Table 1 Configurations of V-groove cylinders

Model	d, mm	h, mm	ϕ, deg	h/d	Re[a]	Re[a]
1	48.2	Smooth	Smooth		$3\times10^5-3.8\times10^5$[b]	
6	48.8	0.60	27	12.3×10^{-3}	$6\times10^4-7.2\times10^4$(?)	$2.6\times10^5-3.1\times10^5$(?)
10	48.8	0.36	44	7.4×10^{-3}		
11	48.8	0.44	23	9.0×10^{-3}	$5.5\times10^4-6.3\times10^4$	$2.7\times10^5-3.2\times10^5$
12	48.8	0.47	26	9.6×10^{-3}	$5.7\times10^4-6.6\times10^4$	$2.5\times10^5-2.9\times10^5$
13	48.8	0.40	29	8.2×10^{-3}	$6.4\times10^4-7.0\times10^4$	$2.5\times10^5-2.8\times10^5$
14	101.0	0.42	28	4.2×10^{-3}	$7.3\times10^4-8.5\times10^4$	$3.0\times10^5-3.5\times10^5$

[a]Approximate Reynolds number range where asymmetry in static pressure distribution was found.
[b]Farell and Blessmann.[13]

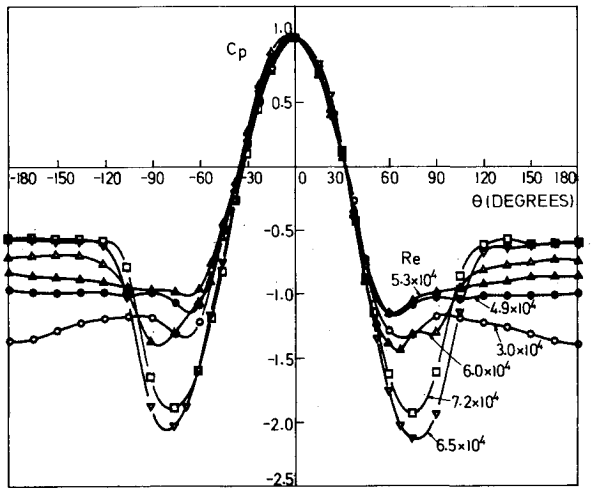

Fig. 3 Pressure distributions on model 11.

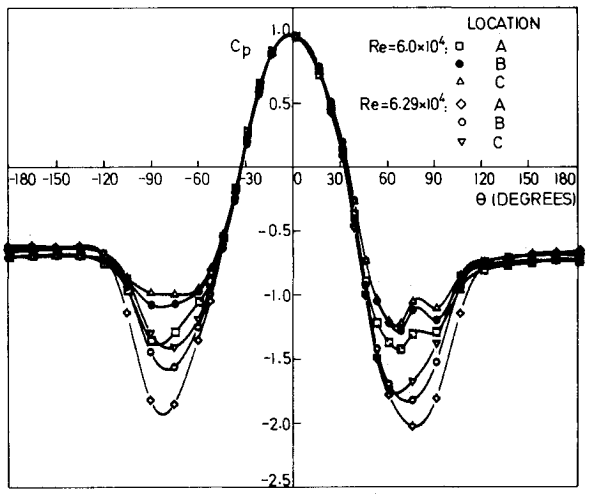

Fig. 4 Spanwise variations of pressure distributions on model 11.

For all the V-groove cylinders, the approximate Reynolds number ranges where asymmetry is found are tabulated in Table 1. Generally, the Reynolds numbers are lower than for the smooth cylinder.[13]

The spanwise variation of the pressure distribution at locations A, B, and C is minimal within the tested Reynolds number range as long as the distribution is symmetric. However, at Reynolds numbers where asymmetry is observed, spanwise variation in the distribution occurs (Fig. 4). At a Reynolds number of 6.3×10^4, the distribution on model 11, including the minimum pressure coefficient C_{pm}, varies significantly. This suggests that there are three-dimensional flow effects. In spite of this, at $Re = 6.0 \times 10^4$, the inflexion point occurs on the same (one) side (only) at all of the spanwise stations over the distance $\Delta z/d = 0.41$.

Integrating these pressure distributions, and others not shown here, gave the drag coefficients C_d shown in Fig. 5. The drag coefficient of the smooth cylinder in the present investigation agrees with that obtained by others within the subcritical regime.[4,5,13,16-18] For the V-groove cylinders, however, the drag coefficient curves are shifted toward lower Reynolds numbers. The drag of model 14 is significantly different from those of the other models. The cause may be due to the difference in V-groove geometry (Table 1). Unfortunately, the Reynolds number range of the wind tunnel is not high enough to define fully the drag minimum for the cylinders of 48.8 mm diameter.

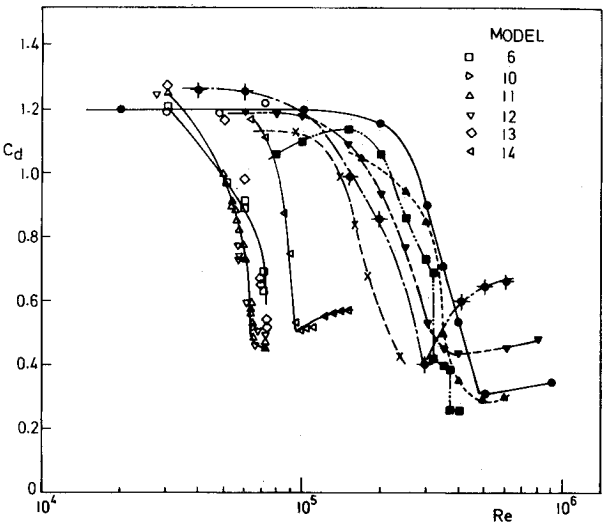

Fig. 5 Drag coefficient of smooth cylinder: ○ present investigation, ● Wieselsberger,[06] ▸ Relf and Simmons,[21] × Fage and Warsap,[17] ◆ Flachsbart,[21] ◂ Drescher,[22] -◆- Achenbach,[18] -■- Bearman,[11] ▲ Guven et al.,[4] ▼ Achenbach and Heinecke,[5] ■ Farell and Blessmann.[13]

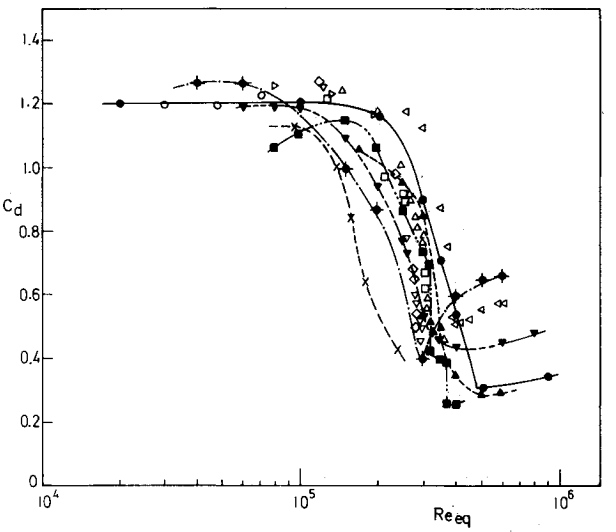

Fig. 6 Variation of drag coefficient with equivalent Reynolds number (symbols as in Fig. 5).

Apparently, the surface geometry is responsible for the difference in critical Reynolds number shown in Fig. 5. For the flow over a smooth cylinder, the drag coefficient is affected by the Reynolds number, surface roughness, wind tunnel blockage, length-to-diameter ratio, freestream turbulence characteristics, and model end conditions. For the V-groove cylinder, however, the presence of the V-grooves introduces an increase in the surface area and thereby possibly an increase of the skin friction, resulting in lower local velocity near the surface. The flow may be similar to the flow in an internally finned channel.[19] An equivalent diameter d_{eq} of the V-groove cylinder can be defined, taking into account the surface area increase caused by the grooves; $d_{eq} = (1 - h/d)d/\sin(\phi/2)$, where $\phi/2$ is the half-angle of the V-groove. Based on this equivalent diameter d_{eq}, the drag coefficients are plotted in Fig. 6 as a function of the equivalent Reynolds number Re_{eq}. Except for model 14, the results for the V-groove cylinders correlate well with those of smooth cylinders obtained by other workers. The deviation of model 14 may be due to its high blockage ratio and low aspect ratio, especially in view of the fact that the correction method of Allen and Vincenti[9] may not be valid within the critical Reynolds number regime.

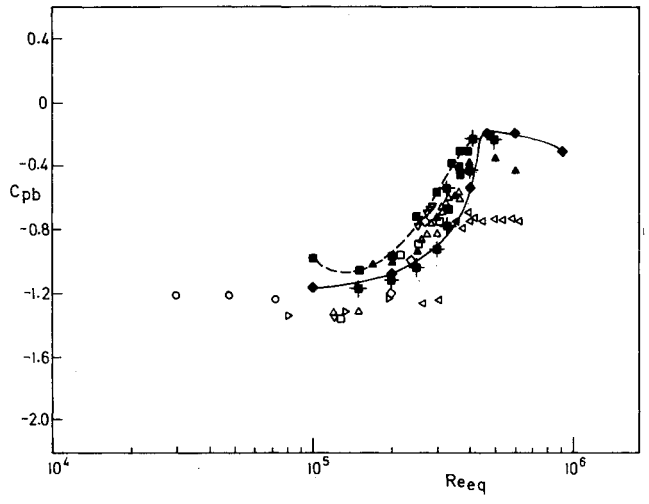

Fig. 7 Variation of base pressure coefficient with equivalent Reynolds number (symbols as in Fig. 5).

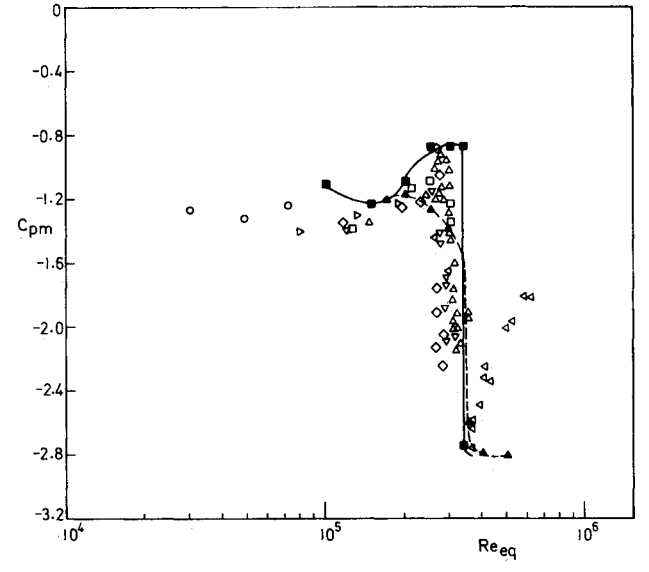

Fig. 8 Variation of minimum pressure coefficient with equivalent Reynolds number (symbols as in Fig. 5).

Using the equivalent Reynolds number Re_{eq}, good correlation is also obtained for C_{pb} and C_{pm} within the subcritical and critical regimes (Figs. 7 and 8). However, within the supercritical regime, no correlation is found. The wide data scatter at $Re_{eq} \approx 3 \times 10^5$ for the V-groove cylinders is caused by the asymmetry in the static pressure distribution and the three-dimensionality of the flow. The correlation of the pressure rise to separation $(C_{pb} - C_{pm})$ is shown in Fig. 9. As has been observed, $(C_{pb} - C_{pm})$ is rather insensitive to the aspect ratio (ℓ/d), tunnel blockage, and end conditions of the test cylinders. Thus, the data scatter is less and the correlation with smooth cylinder results is better than in Figs. 6–8.

The location θ_m of the minimum pressure coefficient and the approximate location θ_w of the beginning of the wake region are shown in Figs. 10 and 11, respectively. Again, the data scatter is due to the asymmetry and three-dimensional flow phenomena within the critical flow regime.

The distribution of the uncorrected Strouhal number St of the vortex shedding is shown in Fig. 12. The abrupt increase of the Strouhal number for the V-groove cylinders occurs at $Re_{eq} \approx 3 \times 10^5$, in agreement with the results for a smooth cylinder at $Re \approx 3 \times 10^5$.

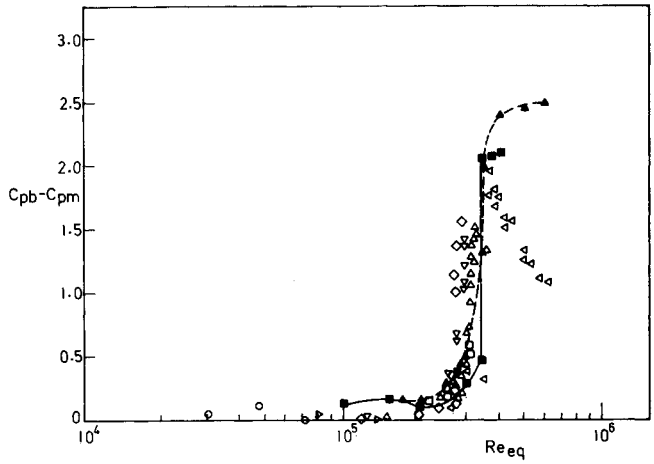

Fig. 9 Variation of $C_{pb} - C_{pm}$ with equivalent Reynolds number (symbols as in Fig. 5).

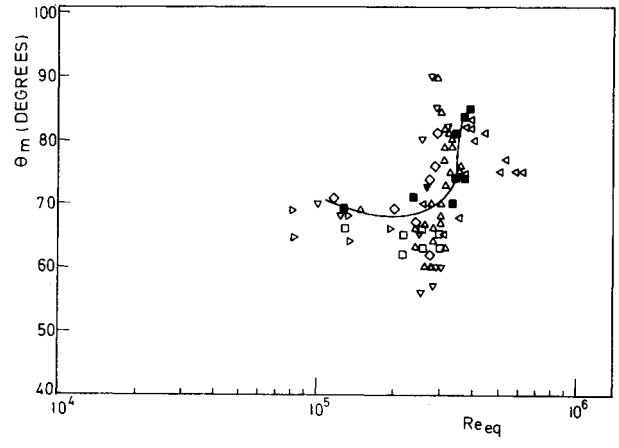

Fig. 10 Variation of θ_m with equivalent Reynolds number (symbols as in Fig. 5).

Detailed measurements of the streamwise u velocity fluctuations of model 11 have been carried out. The spectra at $x/d = 2$, $y/d = 0.5$ are shown in Fig. 13 for different equivalent Reynolds numbers. Distinct spectral peaks are found at $Re_{eq} = 2.45 \times 10^5$ and 3.64×10^5. At $2.80 \times 10^5 \leq Re_{eq} \leq 3.22 \times 10^5$, the spectral peaks are broad or absent. At $Re_{eq} = 3.0 \times 10^5$ ($Re = 6.0 \times 10^4$), the spectral peak is definitely absent. At this equivalent Reynolds number, the static pressure distribution is asymmetric with three-dimensional flow effects and an inflexion point (Figs. 3 and 4). At $Re_{eq} \geq 3.22 \times 10^5$, higher frequency peaks are found. At $3.00 \times 10^5 < Re_{eq} \leq 3.22 \times 10^5$, a single higher frequency peak is present. This is the Reynolds number range where an abrupt drop in the drag coefficient C_d and minimum pressure coefficient C_{pm} occurs and an abrupt increase of $C_{pb} - C_{pm}$ is observed (Figs. 6–9).

The corresponding simultaneous time traces at $x/d = 2$, $y/d = \pm 0.5$ are shown in Fig. 14. Regular time traces are found at $Re_{eq} = 2.45 \times 10^5$ and 3.64×10^5 (Figs. 14a and 14e). At $Re_{eq} = 2.80 \times 10^5$, the time traces become irregular and intermittent on one side of the cylinder (Fig. 14b). At $Re_{eq} = 3.0 \times 10^5$ at which the spectral peak is absent, the occurrence of low-velocity fluctuations simultaneously at the two sides suggests absence of a regular vortex wake during a particular time (Fig. 14c). A similar phenomenon is also found at slightly higher $Re_{eq} = 3.22 \times 10^5$ (Fig. 14d). In other words, at $3.00 \times 10^5 \leq Re_{eq} \leq 3.22 \times 10^5$, unsteady flow oscillations occur at one or the other side of the cylinder, at first intermittently and then in a more regular alternating fashion.

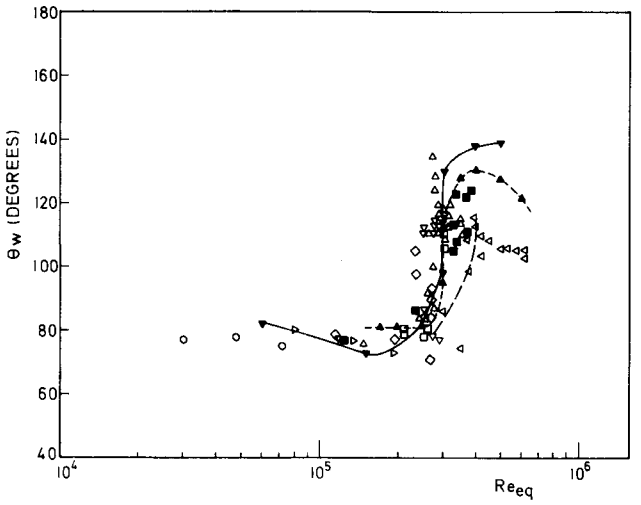

Fig. 11 Variation of θ_w with equivalent Reynolds number (symbols as in Fig. 5).

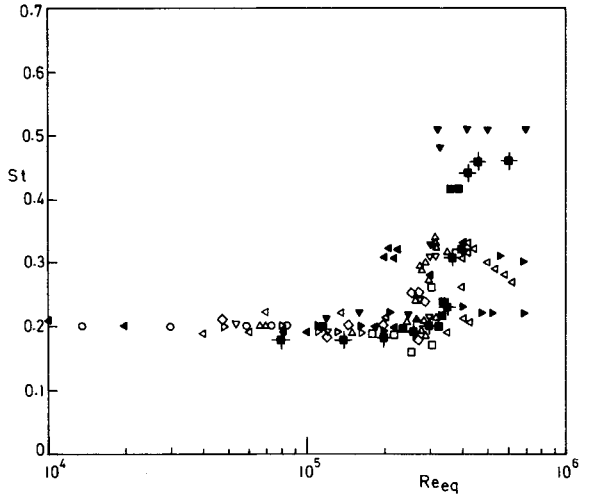

Fig. 12 Variation of Strouhal number (uncorrected) with equivalent Reynolds number (symbols as in Fig. 5).

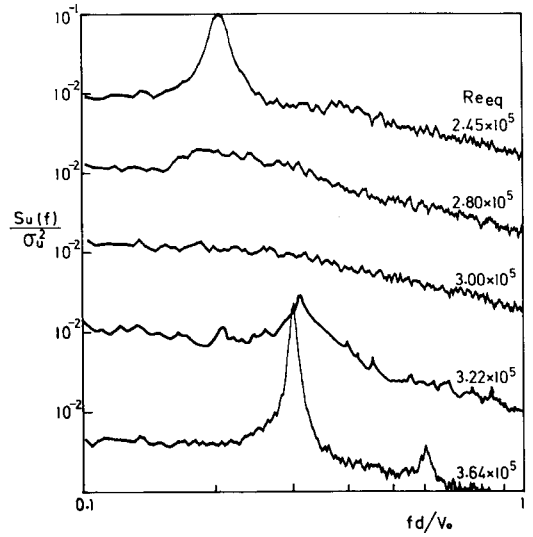

Fig. 13 Spectra of streamwise velocity fluctuations of model 11.

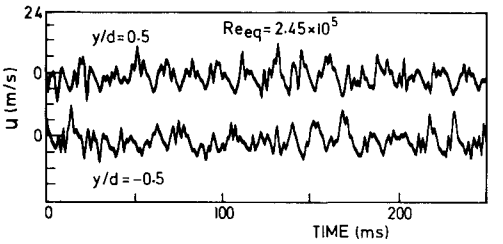

a) $Re_{eq} = 2.45 \times 10^5$.

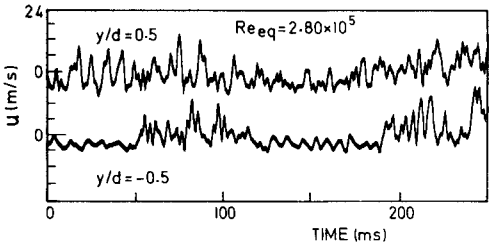

b) $Re_{eq} = 2.80 \times 10^5$.

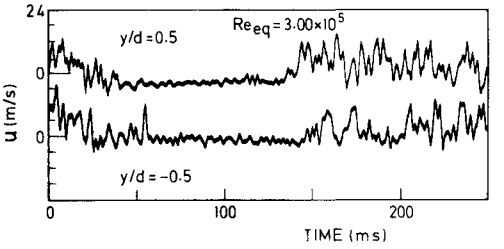

c) $Re_{eq} = 3.00 \times 10^5$.

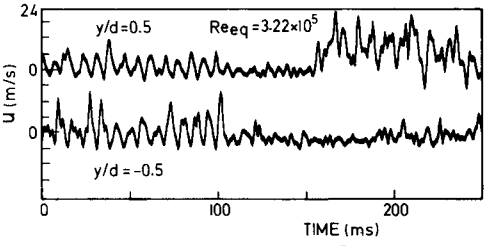

d) $Re_{eq} = 3.22 \times 10^5$.

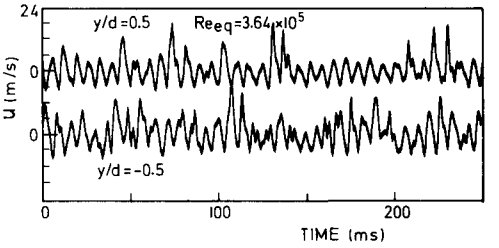

e) $Re_{eq} = 3.64 \times 10^5$.

Fig. 14 Time traces of streamwise velocity at $y/d = \pm 0.5$ of model 11.

The static pressure and velocity fluctuations results discussed above indicate that at $Re_{eq} = 2.45 \times 10^5$ the flow regime is subcritical and it persists up to $Re_{eq} = 2.80 \times 10^5$. It is within this regime that laminar separation is found. Transition from the subcritical to the critical regime of one bubble flow (laminar separation/turbulent reattachment) starts at $Re_{eq} = 3.00 \times 10^5$. The abrupt change in flow characteristics observed indicates that this is the critical equivalent Reynolds number.[11] At $Re_{eq} = 3.22 \times 10^5$, the flow regime with pure one bubble flow geometry is found. It is only at $Re_{eq} = 3.64 \times 10^5$ that transition between one and two bubble flow regimes starts.[13]

For the supercritical flow regime, where $Re_{eq} > 3.5 \times 10^5$, the V-groove cylinder results are those of model 14, with a blockage ratio of 18% and an aspect ratio of 4.4. The blockage

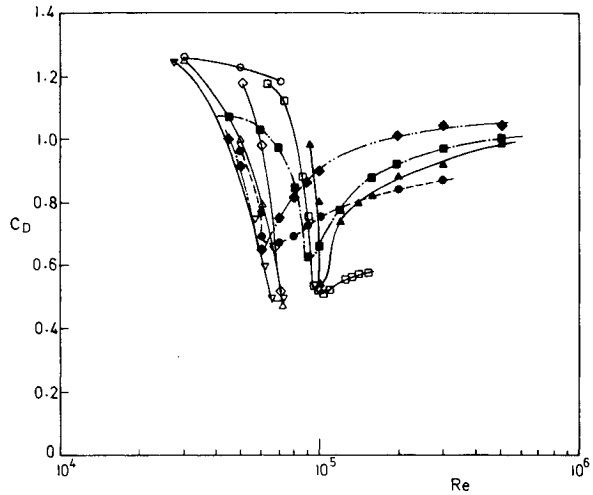

Fig. 15 Comparison of drag coefficient of V-groove and rough cylinders: V-groove cylinder—□ $h/d = 4.2 \times 10^{-3}$, ○ $h/d = 6.2 \times 10^{-3}$, ◇ $h/d = 8.2 \times 10^{-3}$, △ $h/d = 9 \times 10^{-3}$, ▽ $h/d = 9.6 \times 10^{-3}$; Rough cylinder—Achenbach[3]: ■ $k_s/d = 4.5 \times 10^{-3}$, ◆ $k_s/d = 9 \times 10^{-3}$; Guven et al.[4]: ▲ 3.1×10^{-3}; ● Fage and Warsap[17]: $k_s/d = 7 \times 10^{-3}$.

ratio is comparable with that of Achenbach and Heinecke.[5] However, the supercritical uncorrected Strouhal number of the present V-groove cylinder is $0.27 < St < 0.33$, somewhat lower than that of their smooth cylinder, which was $0.4 < St < 0.52$, for blockage ratios of 6–50%.[5] In this regime, no regular vortex wake was found for aspect ratio $\ell/d = 3.38$, but for $\ell/d = 6.75$ a quasiregular Strouhal number of around 0.5 was observed.[5] It has been shown by Theisen[23] that for $\ell/d = 4$ no vortex shedding can exist because the necessary spanwise momentum transfer in the wake cannot take place. Thus, the Strouhal number of about 0.3 for the V-groove cylinder is due to the low aspect ratio, $\ell/d = 4.4$, or to other factors. Once it is formed, the frequency is probably the same as for higher aspect ratios. With this assumption, the appreciably lower Strouhal number would be due to other factors such as the V-groove geometry. Further measurements are needed to determine the exact mechanism involved.

The phenomenon of the shift to lower Reynolds numbers of the different flow regimes of the V-groove cylinder is similar to that of rough cylinders. The drag coefficients of the V-groove cylinder of the same h/d and those of rough cylinders[3,4] of the same k_s/d are shown in Fig. 15. Fairly good agreement between the two sets of results is found in the critical regime. In the supercritical regime, although the present results are of low aspect ratio and high blockage ratio, the drag coefficient of the V-groove cylinder seems to be lower than that of the rough cylinder. The cause is being investigated.

Conclusions

The present experimental results for circular cylinders of different V-groove configurations in the Reynolds number range of 2.0×10^4 to 1.6×10^5 have indicated that, based on the measured aerodynamic characteristics, the flow over these cylinders undergoes earlier transitions from subcritical to critical and from critical to supercritical regimes than a smooth cylinder. By taking into account the added surface area due to the V-grooves, an equivalent diameter of the cylinder can be defined. The equivalent Reynolds number, based on this diameter, provides good correlation of the results for the V-groove cylinders with those of a smooth cylinder within the tested subcritical and critical flow regimes.

References

[1] Walsh, M.J. and Weinstein, L.M., "Drag and Heat-transfer Characteristics of Small Longitudinally Ribbed Surface," *AIAA Journal*, Vol. 17, July 1979, pp. 770–771.

[2] Walsh, M.J., "Drag Characteristics of V-groove and Transverse Curvature Riblets," *AIAA Progress in Astronautics and Aeronautics: Viscous Flow Drag Reduction*, Vol. 72, edited by G.R. Hough, AIAA, New York, 1980, pp. 168–184.

[3] Achenbach, E., "Influence of Surface Roughness on the Cross-flow Around a Circular Cylinder," *Journal of Fluid Mechanics*, Vol. 46, March 1971, pp. 321–335.

[4] Guven, O., Farell, C., and Patel, V.C., "Surface-roughness Effects on the Mean Flow Past Circular Cylinders," *Journal of Fluid Mechanics*, Vol. 98, June 1980, pp. 673–701.

[5] Achenbach, E. and Heinecke, E., "On Vortex Shedding from Smooth and Rough Cylinders in the Range of Reynolds Numbers 6×10^3 to 5×10^6," *Journal of Fluid Mechanics*, Vol. 109, Aug. 1981, pp. 239–251.

[6] Nakamura, Y. and Tomonari, Y., "The Effects of Surface Roughness on the Flow Past Circular Cylinders at High Reynolds Numbers," *Journal of Fluid Mechanics*, Vol. 123, Oct. 1982, pp. 363–378.

[7] Buresti, G., "Appraisal of Universal Wake Numbers from Data for Roughened Circular Cylinders," *Transactions of ASME, Journal of Fluids Engineering*, Vol. 105, Dec. 1983, pp. 464–468.

[8] Schechenyi, E., "Supercritical Reynolds Number Simulation for Two-dimensional Flow over Circular Cylinders," *Journal of Fluid Mechanics*, Vol. 70, Aug. 1975, pp. 529–542.

[9] Allen, H.J. and Vincenti, W.G., "Wall Interference in a Two-dimensional-flow Wind Tunnel with Consideration of the Effect of Compressibility," NACA Rept. 782, 1930.

[10] Niemann, H.J., "On the Stationary Wind Loading of Axisymmetric Structure in the Transcritical Reynolds Number Region," *Institut Konstruktiven Ingenieurban*, Ruhr University, Bochun, FRG, Rept. 71-2, 1971.

[11] Bearman, P.W., "On Vortex Shedding from a Circular Cylinder in the Critical Reynolds Number Regime," *Journal of Fluid Mechanics*, Vol. 37, July 1969, pp. 577–585.

[12] Ericsson, L.E. and Reding, J.P., "Criterion for Vortex Periodicity in Cylinder Wakes," *AIAA Journal*, Vol. 17, Sept. 1979, pp. 1012–1013.

[13] Farell, C. and Blessmann, J., "On Critical Flow Around Smooth Circular Cylinders," *Journal of Fluid Mechanics*, Vol. 136, Nov. 1983, pp. 375–391.

[14] Roshko, A., "Experiments on the Flow Past a Circular Cylinder at Very High Reynolds Number," *Journal of Fluid Mechanics*, Vol. 10, May 1961, pp. 345–356.

[15] Morkovin, M.V., "Flow Around a Circular Cylinder—a Kaleidoscope of Challenging Fluid Phenomena," *Proceedings of ASME Symposium on Fully Separated Flows*, ASME, New York, 1964, pp. 102–118.

[16] Wieselsberger, C., "Neuere Feststellungen uber die Gesetze des Flussigkeits-und Luftwiderstands," *Physikalische Zeitschrift*, Vol. 22, 1921, pp. 321–328.

[17] Fage, A. and Warsap, J.H., "The Effects of Turbulence and Surface Roughness on the Drag of a Circular Cylinder," British Aeronautical Research Council, Rept. 1179, 1929.

[18] Achenbach, E., "Distribution of Local Pressure and Skin Friction Around a Circular Cylinder in Cross-flow up to $Re = 5 \times 10^6$," *Journal of Fluid Mechanics*, Vol. 34, Dec. 1968, pp. 625–639.

[19] Scott, M.J. and Webb, R.L., "Analytic Prediction of the Friction Factor for Turbulent Flow in Internally Finned Channels," *Transactions of ASME, Journal of Heat Transfer*, Vol. 103, Aug. 1981, pp. 423–428.

[20] Relf, E.F. and Simmons, L.F.G., "The Frequency of Eddies Generated by the Motion of Circular Cylinders Through a Fluid," British Aeronautical Research Council, R&M 917, 1924.

[21] Flachsbart, O., "Windruck auf Gasbehalter," *Reports of the Aerodyn. Versuchsanstalt*, IVth Series, Göttingen, FRG, 1932, pp. 134–138.

[22] Drescher, H., "Messung der auf Querangestromte Zylinder Ausgenubten Zeitlich Veranderlichen Drucke.," *Zeitschrift für Flugwissenschaften*, Vol. 4, 1956, pp. 17–21.

[23] Theisen, J.G., "Vortex Periodicity in Wakes," AIAA Paper 67-34, 1967.